WILEY-VCH

Edited by Valentine P. Ananikov

Understanding Organometallic Reaction Mechanisms and Catalysis

Computational and Experimental Tools

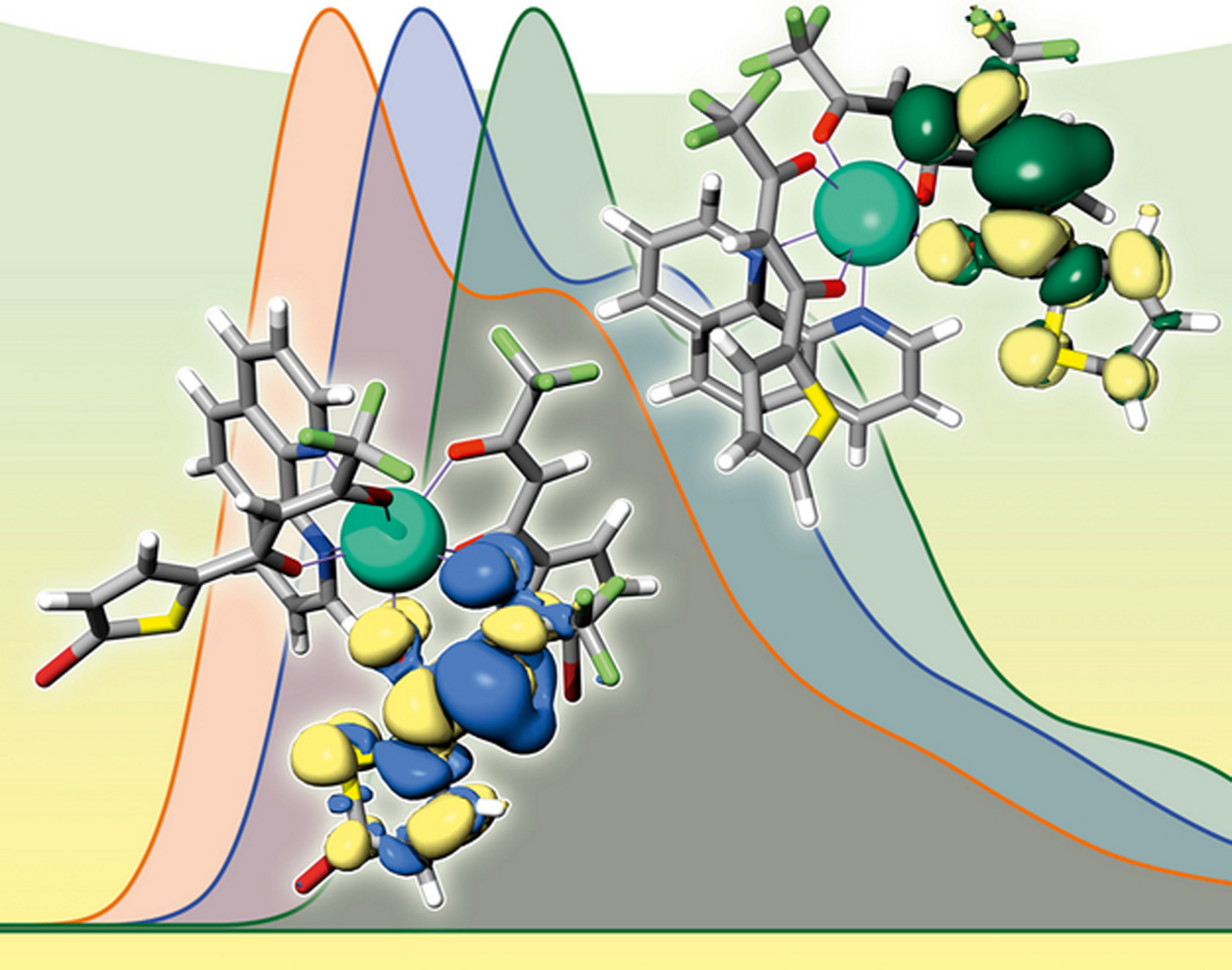

Edited by
Valentine P. Ananikov

Understanding Organometallic Reaction Mechanisms and Catalysis

Related Titles

Ruckenstein, E., Wang, H.

Heterogeneous Catalysis
Experimental and Theoretical Studies

2014
Print ISBN: 978-1-118-54690-1
(Also available in a variety of electronic formats)

Temkin, O.N.

Homogeneous Catalysis with Metal Complexes - Kinetic Aspects and Mechanisms

2012
Print ISBN: 978-0-470-66699-9
(Also available in a variety of electronic formats)

Li, C., Liu, Y. (eds.)

Bridging Heterogeneous and Homogeneous Catalysis
Concepts, Strategies, and Applications

2014
Print ISBN: 978-3-527-33583-1
(Also available in a variety of electronic formats)

Deutschmann, O. (ed.)

Modeling and Simulation of Heterogeneous Catalytic Reactions
From the Molecular Process to the Technical System

2012
Print ISBN: 978-3-527-32120-9
(Also available in a variety of electronic formats)

Beller, M., Renken, A., van Santen, R.A. (eds.)

Catalysis
From Principles to Applications

2012
Print ISBN: 978-3-527-32349-4

Pregosin, P.S.

NMR in Organometallic Chemistry

2012
Print ISBN: 978-3-527-33013-3
(Also available in a variety of electronic formats)

Edited by Valentine P. Ananikov

Understanding Organometallic Reaction Mechanisms and Catalysis

Computational and Experimental Tools

WILEY-VCH
Verlag GmbH & Co. KGaA

The Editor

Prof. Dr. Valentine P. Ananikov
Russian Academy of Sciences, Zelinsky
Institute of Organic Chemistry
47 Leninski Prospect
119991 Moscow
Russia

Library of Congress Card No.: applied for

British Library Cataloguing-in-Publication Data
A catalogue record for this book is available from the British Library.

Bibliographic information published by the Deutsche Nationalbibliothek
The Deutsche Nationalbibliothek lists this publication in the Deutsche Nationalbibliografie; detailed bibliographic data are available on the Internet at <http://dnb.d-nb.de>.

Print ISBN: 978-3-527-33562-6
ePDF ISBN: 978-3-527-67824-2
ePub ISBN: 978-3-527-67822-8
Mobi ISBN: 978-3-527-67823-5
oBook ISBN: 978-3-527-67821-1

Cover-Design Formgeber, Mannheim, Germany
Typesetting Laserwords Private Limited, Chennai, India
Printing and Binding Markono Print Media Pte Ltd, Singapore

Printed on acid-free paper

Contents

List of Contributors

Valentine P. Ananikov
Russian Academy of Sciences
Zelinsky Institute of Organic Chemistry
Leninsky Prospekt 47
Moscow, 119991
Russia

and

Lomonosov Moscow State University
Department of Chemistry
Leninskie Gory
Moscow, 119991
Russia

Vincenzo Barone
Scuola Normale Superiore
Piazza dei Cavalieri 7
Pisa I-56126
Italy

Danila A. Barskiy
International Tomography Center
SB RAS, 3A Institutskaya Street
Novosibirsk, 630090
Russia

and

Novosibirsk State University
Department of Natural Sciences
2 Pirogova Street
Novosibirsk, 630090
Russia

Malgorzata Biczysko
Scuola Normale Superiore
Piazza dei Cavalieri 7
Pisa I-56126
Italy

Ivan Carnimeo
Scuola Normale Superiore
Piazza dei Cavalieri 7
I-56126 Pisa
Italy

Niels Johan Christensen
Technical University of Denmark
Department of Chemistry
Kemitorvet, building 207
Lyngby, DK-2800
Denmark

Ting Fan
The Hong Kong University of Science and Technology
Department of Chemistry
Clear Water Bay
Kowloon
Hong Kong

Natalie Fey
University of Bristol
School of Chemistry
Cantock's Close
Bristol, BS8 1TS
UK

Peter Fristrup
Technical University of Denmark
Department of Chemistry
Kemitorvet, building 207
Lyngby, DK-2800
Denmark

Osvaldo Gutierrez
University of Pennsylvania
Department of Chemistry
Roy and Diana Vagelos Laboratories
231 S. 34 Street
Philadelphia
19104-6323 PA
USA

Igor V. Koptyug
International Tomography Center
SB RAS, 3A Institutskaya Street
Novosibirsk, 630090
Russia

and

Novosibirsk State University
Department of Natural Sciences
2 Pirogova Street
Novosibirsk, 630090
Russia

Kirill V. Kovtunov
International Tomography Center
SB RAS, 3A Institutskaya Street
Novosibirsk, 630090
Russia

and

Novosibirsk State University
Department of Natural Sciences
2 Pirogova Street
Novosibirsk, 630090
Russia

Marisa C. Kozlowski
University of Pennsylvania
Department of Chemistry
Roy and Diana Vagelos Laboratories
231 S. 34 Street
Philadelphia
19104-6323 PA
USA

Sebastian Kozuch
University of North Texas
Department of Chemistry
Center for Advanced Scientific Computing and Modeling (CASaM)
Denton
TX 76203-5070
USA

Robert Kretschmer
Technische Universität Berlin
Institut für Chemie
Straße des 17. Juni 115
Berlin, 10623
Germany

Zhenyang Lin
The Hong Kong University of
Science and Technology
Department of Chemistry
Clear Water Bay
Kowloon
Hong Kong

Daniel Lupp
Technical University of Denmark
Department of Chemistry
Kemitorvet, building 207
Lyngby, DK-2800
Denmark

Jason M. Lynam
University of York
Department of Chemistry
Heslington
York, YO10 5DD
UK

Djamaladdin G. Musaev
Emory University
Cherry L. Emerson Center for
Scientific Computation
1515 Dickey Drive
Atlanta
Georgia 30322
USA

Mikhail V. Polynski
Russian Academy of Sciences
Zelinsky Institute of Organic
Chemistry
Leninsky Prospekt 47
Moscow, 119991
Russia

and

Lomonosov Moscow State
University
Department of Chemistry
Leninskie Gory
Moscow, 119991
Russia

Oleg G. Salnikov
International Tomography
Center
SB RAS, 3A Institutskaya Street
Novosibirsk, 630090
Russia

and

Novosibirsk State University
Department of Natural Sciences
2 Pirogova Street
Novosibirsk, 630090
Russia

Maria Schlangen
Technische Universität Berlin
Institut für Chemie
Straße des 17. Juni 115
Berlin, 10623
Germany

Franziska Schoenebeck
RWTH Aachen University
Institute of Organic Chemistry
Landoltweg 1
Aachen, 52056
Germany

Helmut Schwarz
Technische Universität Berlin
Institut für Chemie
Straße des 17. Juni 115
Berlin, 10623
Germany

Ivan V. Skovpin
International Tomography Center
SB RAS, 3A Institutskaya Street
Novosibirsk, 630090
Russia

and

Novosibirsk State University
Department of Natural Sciences
2 Pirogova Street
Novosibirsk, 630090
Russia

John M. Slattery
University of York
Department of Chemistry
Heslington
York, YO10 5DD
UK

Adrian Varela-Alvarez
Emory University
Cherry L. Emerson Center for Scientific Computation
1515 Dickey Drive
Atlanta
Georgia 30322
USA

Vladimir V. Zhivonitko
International Tomography Center
SB RAS, 3A Institutskaya Street
Novosibirsk, 630090
Russia

and

Novosibirsk State University
Department of Natural Sciences
2 Pirogova Street
Novosibirsk, 630090
Russia

Preface

Understanding electronic structure and reactivity of organometallic compounds remains the problem of fundamental importance in modern chemistry. Development of catalysis and organic chemistry was largely governed by elucidation of reaction mechanisms and utilization of this knowledge to control selectivity and improve yields in synthetic applications dealing with medicinal chemistry, preparation of pharmaceutical and biologically active molecules, industrial processes, fine organic synthesis, new generation of smart materials and organic electronics. In recent decades research in these areas was stimulated by rapid progress in quantum chemistry and utilization of theoretical calculations to reveal correlations between molecular structure, properties, and reactivity.

Theoretical calculations using modern quantum chemical methods provided an outstanding opportunity to make a valuable insight into the problem and allowed reliable description of reaction mechanisms in catalysis from the first principles. Application of informative and flexible computational procedures on numerous examples has demonstrated accurate computational modeling – often within the accuracy achieved in experimental measurements.

Not surprisingly, there is a remarkable interest in modern experimental chemistry to understand computational methods and to apply these methods in the everyday research. In fact, the number of publications that contain both – experiment studies and theoretical calculations – was tremendously increased over the last years. It is not uncommon for purely experimental research groups to learn theoretical methods and facilitate mechanistic studies, especially in the fields where experimental capabilities alone are not sufficient to solve the problem. Rapid increase in the computational power of modern personal computers and easy availability of high performance CPUs even further stimulate this tendency. What is important nowadays, is to transfer the knowledge about state-of-the-art theoretical methods and fascinating opportunities they open in the studies of transition metal chemistry and catalysis.

The role of this book is to highlight new horizons in the studies of reaction mechanisms that open joint application of experimental studies and theoretical calculations. The book is aimed to provide first hand experience from known

experts that are practically familiar with such complex studies involving both computational and experimental tools.

The present book chapters review organometallic and catalytic reactions in the gas phase, model systems for studying reactions in solution under homogeneous conditions with soluble metal complexes, as well as complex chemical transformations involving heterogeneous systems. Few chapters are dedicated to describe methodology of computational studies for exploration of catalytic cycles and mechanisms of organometallic reactions.

I would like to express my great thanks to the authors that accepted to contribute to the book for their excellent chapters. Finally, I thank Anne Brennfuehrer and Lesley Belfit from Wiley for continuous help and assistance during development of this book project.

Moscow, Russia, 2014 *Valentine Ananikov*

1
Mechanisms of Metal-Mediated C–N Coupling Processes: A Synergistic Relationship between Gas-Phase Experiments and Computational Chemistry

Robert Kretschmer, Maria Schlangen, and Helmut Schwarz

1.1
Introduction

As a consequence of the key positions that the elements carbon and nitrogen occupy in nature, C–N bond formation constitutes an important issue in the synthesis of various products ranging from chemical feedstocks to pharmaceuticals. Not surprisingly, over the last few decades, intensive research has been devoted to this timely topic [1], and the use of ammonia as a relatively inexpensive reagent for C–N coupling reactions has been found to be highly desirable [2]. However, despite the impressive progress reported on the development of new synthetic methodologies, there exists a lack of information on the precise, atomistic-level derived mechanisms in particular for the metal-mediated formation of nitrogen-containing organic molecules generated directly from ammonia. One way to gain such insight is to perform gas-phase experiments on "isolated" reactants. These studies provide an ideal arena for probing experimentally the energetics and kinetics of a chemical reaction in an unperturbed environment at a strictly molecular level without being obscured by difficult-to-control or poorly defined solvation, aggregation, counterion, and other effects. Thus, an opportunity is provided to reveal the intrinsic feature(s) of a catalyst, to explore directly the concept of single-site catalysts, or to probe in detail how mechanisms are affected by factors such as cluster size, different ligands, dimensionality, stoichiometry, oxidation state, degree of coordinative saturation, and charge state. In short, from these experiments, one may learn what determines the outcome of a chemical transformation [3]. In addition, thermochemical and kinetic data derived from these experiments provide a means to benchmark the quality of theoretical studies.

While the study of "naked" gas-phase species will, in principal, never account for the precise kinetic and mechanistic details that prevail at a surface, in an enzyme, or in solution, when complemented by appropriate, computationally derived information, these gas-phase experiments prove meaningful on the ground that they permit a systematic approach to address the above-mentioned questions; moreover, they provide a conceptual framework. The DEGUSSA process, which is the rather unique, platinum-mediated, large-scale coupling of CH_4

Understanding Organometallic Reaction Mechanisms and Catalysis: Computational and Experimental Tools, First Edition. Edited by Valentine P. Ananikov.

and NH_3 to generate HCN [4], serves as a good example. Mass spectrometry-based experiments [5a] suggested both the key role of CH_2NH as a crucial gas-phase transient and also pointed to the advantage of using a bimetallic system rather than a pure platinum-based catalyst for the C–N coupling step to diminish undesired, catalyst-poisoning "soot" formation [6, 7]. The existence of CH_2NH was later confirmed by *in situ* photoionization studies [8] and catalysts that are currently employed contain silver-platinum alloys rather than pure platinum.

In this chapter, we focus on two types of gas-phase C–N coupling processes, Eqs. (1.1) and (1.2), using metal complexes bearing simple carbon- and nitrogen-based ligands and probing their thermal reactions with ammonia and hydrocarbons, respectively. While we will refrain from describing the various experimental techniques and computational methods or the way the reactive species $[M(CH_x)]^+$ and $[M(NH_x)]^+$ are generated [9], the emphasis will rather be on the elucidation of the often intriguing mechanisms of these metal-mediated coupling reactions.

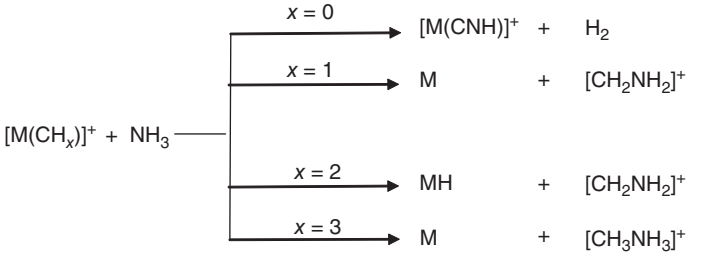

(1.1)

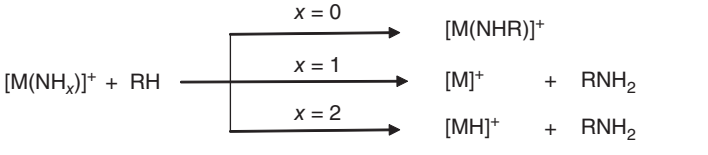

(1.2)

1.2
From Metal-Carbon to Carbon–Nitrogen Bonds

1.2.1
Thermal Reactions of Metal Carbide and Metal Methylidene Complexes with Ammonia

The major ionic product in the reactions of $[Pt_n(C)]^+$ ($n = 1, 2$) with NH_3 corresponds to dehydrogenation of the latter [10]. While there is no direct spectroscopic support for the structure assignment of the generated $[Pt_n(C,N,H)]^+$ ions, circumstantial evidence is provided by the ion/molecule reaction of the mass-selected product ions $[Pt(C,N,H)]^+$ with NH_3, Eq. (1.3).

(1.3)

$$[Pt_2(C,N,H)]^+ + NH_3 \not\longrightarrow [Pt_2(NH_3)]^+ + HCN \quad (1.4)$$

Occurrence of reaction (1.3) suggests the presence of a preformed HCN (or HNC) ligand in $[Pt(C,N,H)]^+$. Thus, in contrast to $[Pt_2(C,N,H)]^+$, generated from $[Pt_2C]^+$ and not being able to release HCN, Eq. (1.4), the mononuclear platinum carbide $[Pt(C)]^+$ induces C–N bond formation upon reaction with NH_3; apparently, this species serves as one of the late reactive intermediates to generate HCN from CH_4 and NH_3 [5a].

In the thermal ion/molecule reactions of the singlet platinum methylidene clusters $[Pt_n(CH)]^+$ ($n = 1, 2$) with NH_3, the dominant path corresponds to proton transfer to generate $[NH_4]^+$ [11]. In addition, for the mononuclear precursor, the couple $[Pt(CH)]^+/NH_3$ gives rise to the formation of $[CH_2NH_2]^+$ concomitant with the loss of atomic platinum; clearly, transfer to and insertion of the electrophilic CH^+ unit in a N–H bond of ammonia provides the methane iminium ion $[CH_2NH_2]^+$.

This reaction, Eq. (1.1) with $x = 1$, has also been studied in quite some detail for the group 10 systems $[M(CH)]^+/NH_3$ (M = Ni, Pd, Pt), and remarkable metal-dependent differences have been noted [3j]. For the couples $[M(CH)]^+/NH_3$ (M = Ni, Pt),[1] the following branching ratios were obtained, Eq. (1.5); mechanisms of the various processes were uncovered by extensive density functional theory (DFT) calculations and deuterium-labeling experiments employing $[M(CD)]^+/NH_3$ and $[M(CH)]^+/ND_3$ [3j].

			Ni	Pt
$[M(CH)]^+ + NH_3$	→ $[CH_2NH_2]^+ + M$		37%	51%
	→ $[M(C,N,H_2)]^+ + H_2$		18%	35%
	→ $[M(CHNH_2)]^+ + H$		45%	-
	→ $[NH_4]^+ + MC$		-	14%

(1.5)

Proton transfer to produce $[NH_4]^+$ and the neutral metal carbide MC is exothermic only for M = Pt as a consequence of the relatively small proton affinity (PA) of 780 kJ mol^{-1} for PtC as compared with $PA(NH_3) = 852$ kJ mol^{-1}; in contrast, $PA(NiC) = 915$ and $PA(PdC) = 879$ kJ mol^{-1} are too high to let $[M(CH)]^+$ act as a Brønsted acid toward NH_3.

Further, the elimination of a hydrogen atom, originating exclusively from the incoming ligand NH_3, to generate eventually the amino-substituted metal carbene complex $[M(CHNH_2)]^+$ reflects thermochemical features. Specifically, the M–H bond strength of the central intermediate $[H–M(CHNH_2)]^+$ increases from nickel

1) While experiments had to be confined to M = Ni and Pt due to the fact that the Pd complexes could not be generated, extensive DFT calculations were performed for all three group 10 systems.

to platinum such that the reaction is exothermic for nickel but endothermic for the other two-metal complexes.

Clearly, C–N bond formation is also involved in the generation of $[CH_2NH_2]^+$ as well as in the dehydrogenation paths to produce either $[M(CHNH)]^+$ or isomeric $[M(CNH_2)]^+$. Depending on the metal, these two isomers are formed via different mechanisms; while for nickel and palladium, a σ-bond metathesis is operative, for platinum a sequence of oxidative addition/reductive elimination is involved [12]. In addition, in the formation of $[CH_2NH_2]^+$, the actual mechanism of the intracomplex hydrogen rearrangement, that is, a direct [1.2] migration versus a metal-mediated hydrogen transfer is quite affected by the electronic structure of the intermediate $[M(CH–NH_3)]^+$ [3j].

1.2.2
How Metals Control the C–N Bond-Making Step in the Coupling of CH_4 and NH_3

Under thermal conditions, the system $[Pt]^+/CH_4/NH_3$ reacts with 76–80% efficiency [5] relative to the collision rate, to form $[Pt(CH_2)]^+$; dehydrogenation of ammonia by atomic Pt^+ to produce $[Pt(NH)]^+$ is endothermic [5a, 13]. Further, if independently generated $[Pt(NH)]^+$ is reacted with CH_4, the products $[Pt(CH_2)]^+$ and NH_3 are mainly formed (85%), presumably in a σ-metathesis process with $[CH_2NH_2]^+/PtH$ (10%), and $[Pt(CNH)]^+/2H_2$ (5%) generated as by-products. Thus, it is the metal carbene complex $[Pt(CH_2)]^+$ that serves as the key intermediate in the C–N coupling of CH_4 and NH_3. As shown in Eq. (1.6), in addition to minor proton transfer to generate $[NH_4]^+$, the two major products are associated with the formation of C–N bonds. On the basis of labeling experiments, both $[CH_2NH_2]^+$ and $[Pt(CHNH_2)]^+$ are formed in clean reactions in which $[Pt(CH_2–NH_3)]^+$ serves as the central precursor. As mentioned, extensive labeling experiments complemented by DFT calculations shed light on the mechanisms of the reactions [5].

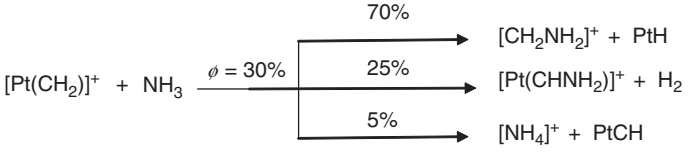

(1.6)

As shown in Figure 1.1, in the dehydrogenation of intermediate **3**, which is also accessible in a detour $\mathbf{1} + NH_3 \rightarrow [H_3N–Pt–CH_2]^+$ (**2**) → **3**, the platinum center is exploited as a "catalyst." According to DFT calculations, the sequence of metal-mediated N–H and C–H bond activations to generate **6** is energetically favored over the alternative path commencing with a C–H bond activation (**3** → **5** → **6**). The metal-free, symmetry-forbidden [1.2] hydrogen migration/elimination path (**3** → **7**) is significantly higher in energy and not accessible under ambient conditions.

C–N coupling in the thermal reactions of $[M(CH_2)]^+$ with NH_3 is not confined to M = Pt. While the carbenes of the 3d metals $[Fe]^+$ and $[Co]^+$ are

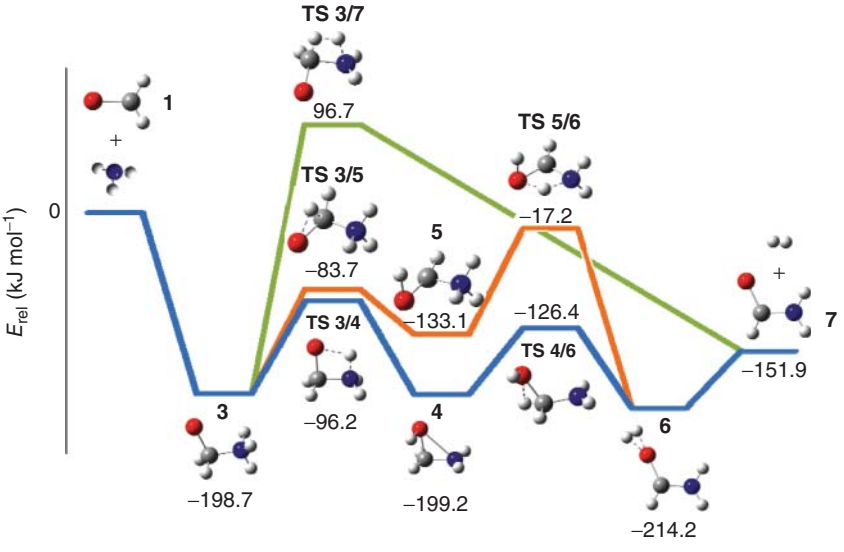

Figure 1.1 Simplified potential-energy surface (PES) of the reaction $[Pt(CH_2)]^+/NH_3 \rightarrow [Pt(CHNH_2)]^+/H_2$ calculated for the doublet spin surface at the B3LYP/TZP//B3LYP/DZP level; relative energies are given in kJ mol^{-1} and are corrected for zero-point vibrational energies. For the sake of clarity, charges are omitted. Color code: red platinum, gray carbon, blue nitrogen, white hydrogen. (Adapted from Ref. [5a]. Copyright American Chemical Society, **1999**.)

completely unreactive toward ammonia, those of the 4d and 5d metals, Rh, W, Os, and Ir, exhibit moderate efficiencies (10–40% of the collision rate). The major pathway in the reaction of $[Rh(CH_2)]^+$ and NH_3 yields $[Rh]^+$, a product channel that is not observed for any of the carbene complexes studied. On thermochemical grounds, the neutral molecule produced can only correspond to CH_3NH_2 and its formation requires metals with $D_0(M^+–CH_2) < 364\,kJ\,mol^{-1}$; this requirement is met for $[Rh(CH_2)]^+$ ($D_0 = 355\,kJ\,mol^{-1}$) but for none of the 5d metal carbene precursors. For the complexes of osmium and iridium, large fractions of the metal carbenes are consumed by simple acid-base reactions with ammonia to afford neutral MCH species. It remains to be established whether this is a consequence of the fact that dehydrogenation of methane by $[Os]^+$ and $[Ir]^+$ gives rise to a hydrido-methylidene complex $[M(H)(CH)]^+$ (M = Ir, Os) rather than the conventional carbene isomer $[M(CH_2)]^+$ [5c,d]. The behavior of the couple $[Au(CH_2)]^+/NH_3$ is rather unique. With an efficiency of 60%, the only product pair generated corresponds to $[CH_2NH_2]^+$ and neutral AuH. The branching ratio of aminocarbene versus metal hydride formation reflects directly the reaction enthalpies ($\Delta_r H$) for the formations of $[CH_2NH_2]^+$ and neutral MH, which themselves depend on $D_0(M^+–CH_2)$ versus $D_0(M–H)$. $\Delta_r H$ amounts to $-180\,kJ\,mol^{-1}$ for the $[Au(CH_2)]^+/NH_3$ couple and to only $-84\,kJ\,mol^{-1}$ for the platinum system.

In contrast to the reactions of some of the mononuclear carbene-cluster ions $[M(CH_2)]^+$, no C–N bond coupling is achieved when the carbene complexes of the larger homonuclear cluster ions $[Pt_n(CH_2)]^+$ ($n = 2–5$) or most of the heteronuclear cluster carbenes $[Pt_nM_m(CH_2)]^+$ ($m + n \leq 4$; M = Cu, Ag, Au) are employed [6]; rather, dehydrogenation of the carbene unit, resulting in carbide ("soot") formation, takes place, Eq. (1.7) for $[Pt_n(CH_2)]^+$.

$$[Pt_n(CH_2)]^+ + NH_3 \rightarrow [Pt_n(C)(NH_3)]^+ + H_2 \tag{1.7}$$

$$[PtM(CH_2)]^+ + NH_3 \rightarrow [PtM(CHNH_2)]^+ + H_2 \tag{1.8}$$

However, the heteronuclear complexes $[PtM(CH_2)]^+$ (M = Cu, Ag, Au) exhibit an extraordinary cooperative effect in enhancing C–N coupling at the expense of carbide formation [6, 14], Eq. (1.8). In these bimetallic cluster ions, the platinum core brings about methane activation where relativistic effects [15a] matter, to form a strong metal carbon multiple bond in $[Pt(CH_2)]^+$ [15b]. The role of the coinage metal M in these clusters is to control the branching ratio between unwanted "soot" formation and C–N coupling, demonstrating that, at a strictly molecular level, cooperative effects in heteronuclear cluster catalysis seem to exist. Further insight into mechanistic aspects of this remarkable observation has been provided by relativistic DFT calculations [16]. Accordingly, for the homonuclear system, the cyclic structure **8** (Scheme1.1) is 103.7 kJ mol^{-1} more stable than its acyclic isomer **9**; moreover, the barrier it takes to bring about isomerization **8** → **9** amounts to 118 kJ mol^{-1}. Thus, under the experimental conditions, the only isomer that plays a role in the reaction with NH_3 is **8** (M = Pt). Further, an analysis of the reaction profile for the homonuclear couple $[Pt_2(CD_2)]^+/NH_3$ reveals that the "carbide path" to form **10** and D_2, Scheme 1.1, is energetically favored over the sequence **8** → **9** → **11**. In contrast, for the heteronuclear cluster ions (M = Cu, Ag, and Au), the isomers **8** and **9** are much closer in energy and the barriers for their interconversion are relatively small. In addition, the C–N coupling path **9** → **11** is energetically favored over the generation of the cyclic carbide complex **10**.

1.2.3
C–N Coupling via S_N2 Reactions: Neutral Metal Atoms as a Novel Leaving Group

While $[M(CH_3)]^+$ complexes (with M being a first-row transition metal) do not bring about a reaction according to Eq. (1.9), "bare" $[Zn(CH_3)]^+$ does react with ammonia under ambient conditions. The reaction yields N-protonated methylamine with *neutral atomic* zinc serving as a leaving group, as shown in Figure 1.2 [17].

$$[M(CH_3)]^+ + NH_3 \rightarrow [CH_3NH_3]^+ + M \tag{1.9}$$

A more thorough investigation revealed that this novel gas-phase S_N2-reaction is not confined to zinc but is typical for the whole zinc triad exhibiting both commonalities and differences with regard to the nature of M.

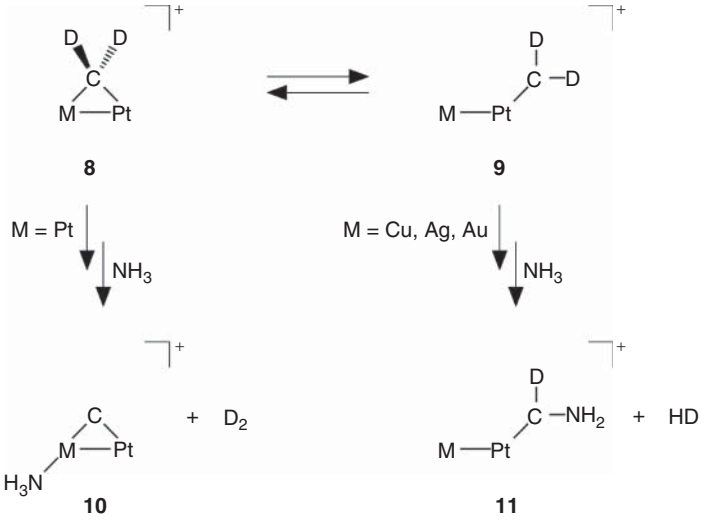

Scheme 1.1 Carbide formation versus C–N coupling in the thermal ion/molecule reactions of $[PtM(CD_2)]^+$ with NH_3 (M = Pt, Cu, Ag, Au).

On the basis of detailed UCCSD(T)/def2-QZVP//UB3LYP/def2-QZVP calculations, the alternative reaction channel in terms of a metathesis reaction under formation of methane, Eq. (1.10), does not occur for M = Zn, Cd, Hg as the result of a kinetic barrier preventing the reaction to proceed under quasi-thermal conditions.

$$[M(CH_3)]^+ + NH_3 \rightleftharpoons [M(NH_2)]^+ + CH_4 \qquad (1.10)$$

Rather, the S_N2 process according to Eq. (1.9) occurs with varying efficiencies of 5.0 (M = Zn), 2.3 (Cd), and 20.4% (Hg). These differences in reactivity parallel the variation of the ionization energies and the calculated methyl-cation affinities (MCAs) of M. The highest efficiency is observed for the most noble metal (i.e., Hg) which at the same time exhibits the smallest MCA. For the liberation of atomic M in the C–N coupling, Eq. (1.9), two pathways were identified computationally that branch out right from the beginning (Figure 1.3): NH_3 can directly coordinate (i) to the metal center (**13a**) or (ii) to the carbon atom of the methyl group (**13b**). Not surprisingly, the gain in complexation energy is much higher for the former path. Next, the encounter complexes **13a,b** react in two different stereochemical modes. In the transition structures **TS 13a/14a**, the M–C bond is largely stretched in comparison to **13a**, and NH_3 attacks the methyl group side-on with retention of configuration at the carbon center. Under thermal conditions, this reductive elimination path is not accessible for any of these metals, as energy values ranging from 57.7 kJ mol^{-1} (for Cd) to 181.2 kJ mol^{-1} (for Hg) above the entrance channel are necessary to achieve **TS 13a/14a**. In contrast, the transition structures **TS 13b/14b** associated with inversion of configuration of the methyl

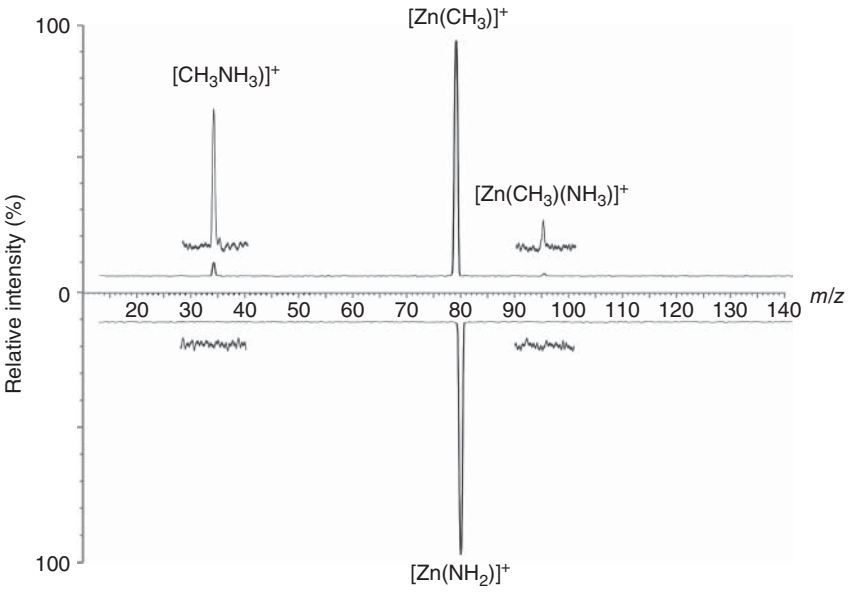

Figure 1.2 Ion/molecule reactions of mass-selected $[Zn(CH_3)]^+$ with NH_3 (upper part), and $[Zn(NH_2)]^+$ with CH_4 (lower part, mirrored at the base line) under thermal conditions. Important regions are enlarged by a factor of 10. (Adapted from Ref. [17]. Copyright WILEY-VCH, **2011**.)

group are located *below* the entrance channel. It is this path that permits, under ambient conditions, a gas-phase S_N2 reaction with a *neutral atomic metal* serving as a leaving group in the C–N coupling reaction; here, the metal M is reduced from the formal oxidation state II to 0. All experimental findings, for example, relating the rate efficiencies with the metal-cation affinities, or the first and second ionization energies of M, are in excellent agreement with the picture of the potential-energy surface (PES) given in Figure 1.3 [18].

1.3 From Metal-Nitrogen to Carbon-Nitrogen Bonds

1.3.1 High-Valent Iron Nitride and Iron Imide Complexes

As already mentioned in Section 1.2, ion/molecule reactions of species having metal-nitrogen bonds with hydrocarbons give rise to the formation of C–N bonds. In this chapter, this topic will be pursued in a more systematic way, and we will commence with a discussion of a high-valent iron-nitrido dication. This field of "iron chemistry" has gained quite some interest over the last decade [19] as a result of their role in metalloenzymatic transformations [20].

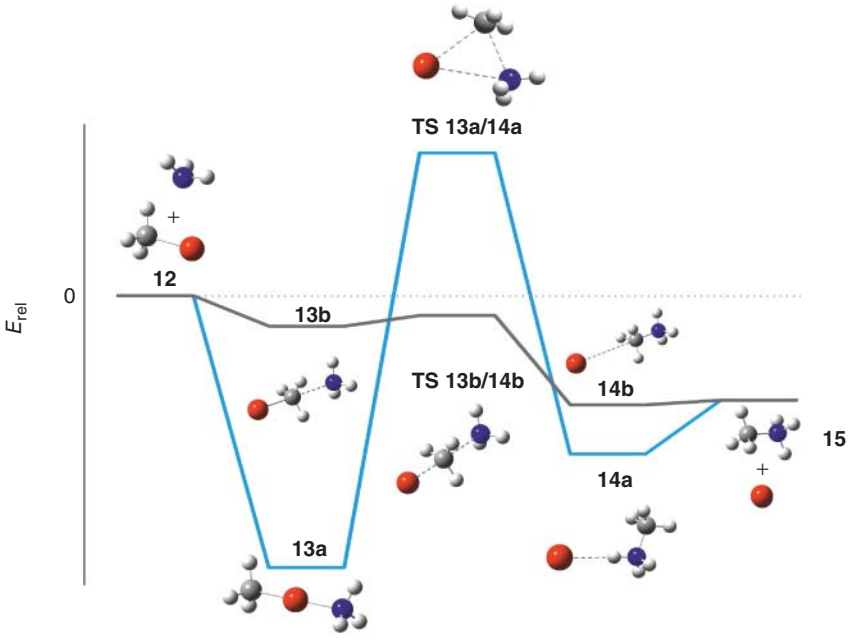

Figure 1.3 Generic PES (singlet ground state) for C–N bond formation to produce $[CH_3NH_3]^+/M$ for the couple $[M(CH_3)]^+/NH_3$ (M = Zn, Cd, Hg); for the sake of clarity, charges are omitted. Color code: red metal, gray carbon, blue nitrogen, white hydrogen. (Adapted from Ref. [18]. Copyright American Chemical Society, **2012**.)

As depicted in Scheme 1.2, the high-valent dication **17** can be generated by collision-induced oxidative N_2 loss from the azido precursor **16** in the gas phase [21] and has been characterized by gas-phase IR spectroscopy of a ^{15}N-labeled isotopologue in conjunction with DFT calculations (M. Schlangen, J.P. Boyd, O. Dopfer, J. Oomens, A. Grohmann, P. Hildebrandt, unpublished results). **17** is not only capable of bringing about suicidal intraligand insertion of the nitride nitrogen atom in C–C, C–H, and N–H bonds (**17** → **18**) or the transfer of a nitrogen atom to a diene unit (**17** → **19** → **20**) [21] but also what is most unusual and unprecedented – the room-temperature nitrile-alkyne metathesis **17** → **21** to generate RCN [22], Scheme 1.2. Here, most likely a sequence of electrophilic addition of the nitrido atom to the C≡C bond, followed by a series of electrocyclic isomerizations is operative (G. Frenking private communication to H. Schwarz).

Early transition-metal imides $[M(NH)]^+$ have bond-dissociation energies large enough that for M = Sc, Ti, V, Y, Zr, Nb, La, and Ta, thermal dehydrogenation of ammonia by $[M]^+$ is possible [23]. A direct and unfortunate consequence of these high bond energies, that is, $D_0(M^+–NH) > 423\,kJ\,mol^{-1}$, is that the $[M(NH)]^+$ species of the early transition metals are featured by a rather low reactivity as far as the transfer of the NH unit to a substrate is concerned. On the other hand,

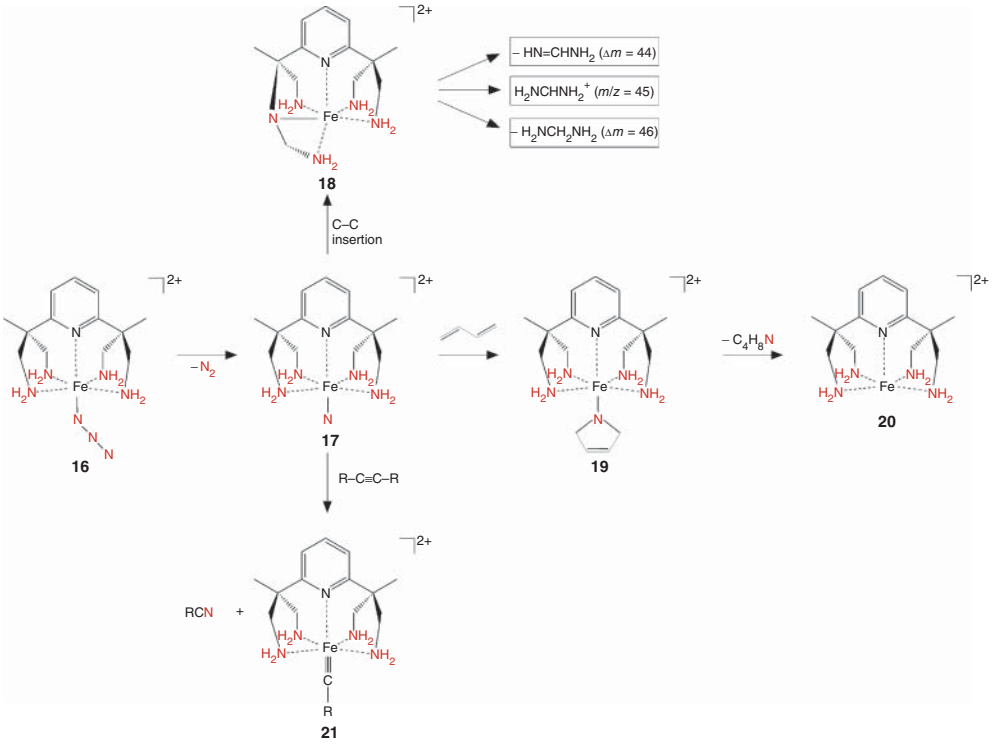

Scheme 1.2 Intra- and intermolecular C–N bond formation involving a high-valent iron-nitrido dication. (Adapted from Ref. [3g]. Copyright WILEY-VCH, **2012**.)

the late 3d transition-metal cations $[Co]^+$, $[Ni]^+$, and $[Cu]^+$ differ in that even at elevated kinetic energies, they do not form the corresponding $[M(NH)]^+$ species when reacted with NH_3 owing to their weak metal-nitrogen bonds [24]. However, $[Fe(NH)]^+$ is expected to possess a well-balanced bonding situation between these extremes along the 3d series, rendering it a suitable candidate for catalytic procedures. This was demonstrated by pioneering work of Freiser and coworkers [25] on the gas-phase reactions of $[Fe(NH)]^+$ with benzene and ethene. This work has since been extended to other substrates and the experimental findings were complemented by electronic structure calculations [26]. $[Fe(NH)]^+$ can also be conveniently generated, for example, in the reactions of $[FeO]^+$ with NH_3 or of bare $[Fe]^+$ with either HN_3 (liberation of N_2) or NH_2OH (loss of H_2O). When mass-selected $[Fe(NH)]^+$ is reacted with hydrocarbons the following findings are worth mentioning:

1) $[Fe(NH)]^+$ is capable to activate CH_4 by insertion of NH in the C–H bond to afford atomic $[Fe]^+$ concomitant with neutral CH_3NH_2. However, the reaction efficiency is surprisingly small ($\varnothing = 0.2\%$) as is the intermolecular kinetic isotope effect KIE = 1.3 derived from the ion/molecule reaction of $[Fe(NH)]^+$ with CD_4.

2) In the much more efficient reactions with C_2H_6 ($ø = 45\%$) and C_3H_8 ($ø = 50\%$), generation of $[Fe]^+$ (with 10 and 5% branching ratios, respectively) is indicative of C–N formation most likely to generate the neutral amines of $C_2H_5NH_2$ and $C_3H_7NH_2$.
3) When $[Fe(NH)]^+$ is reacted with benzene ($ø = 70\%$), the major channel affords ionized aniline and also the other, two minor routes also indicate the operation of C–N coupling processes, Eq. (1.11).

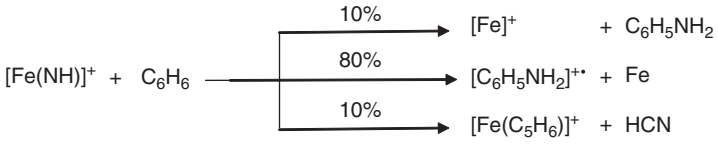

(1.11)

The preference for generating $[C_6H_5NH_2]^{+\bullet}$ versus $[Fe]^+$ is in line with the lower ionization energy (*IE*) of aniline (7.72 eV) versus *IE*(Fe) = 7.87 eV.
4) The thermal reaction of $[Fe(NH)]^+$ with toluene occurs at the collision limit ($ø = 100\%$). Dehydrogenation dominates the product spectrum (85% branching ratio) most likely generating an iron complex bearing a benzylideneamine unit, that is, $C_6H_5CHNH/[Fe]^+$; the C–N coupling product $[C_7H_7NH_2]^{+\bullet}$ amounts to only 5% and, on the basis of a comparison of the *IE*s, corresponds to ionized toluidine rather than benzylamine.

In summary, for most organic substrates, at least partial C–N bond coupling is accomplished by $[Fe(NH)]^+$, which has emerged as a model system for the examination of transition metal–mediated imine transfer in the gas phase.

1.3.2
Metal-Mediated Hydroamination of an Unactivated Olefin by $[Ni(NH_2)]^+$

The atom-economic addition of NH_3 to unactivated olefins is hampered by various obstacles, and in view of the importance of this hydroamination reaction, enormous efforts have been undertaken to develop metal-based catalytic routes [27].

A "room-temperature" variant of this process has been realized in the ion/molecule reaction of the "bare" amidonickel cation $[Ni(NH_2)]^+$ (**22**), which can be generated in the gas phase by reacting $[Ni(OH)]^+$ with NH_3 or by collision-induced dissociation of ESI-generated $[Ni(formamide)_3]^{2+}$ [28].

As shown in Figure 1.4, the thermal reaction of mass-selected $[Ni(NH_2)]^+$ (**22**) with C_2H_4 results in the formation of two primary products, Eqs. (1.12) and (1.13), with a branching ratio of 3.1:1 and an efficiency of $ø = 18\%$.

$$[Ni(NH_2)]^+ + C_2H_4 \rightarrow [C_2H_6N]^+ + Ni \quad (1.12)$$

$$[Ni(NH_2)]^+ + C_2H_4 \rightarrow [Ni(C_2H_4N)]^+ + H_2 \quad (1.13)$$

The assignment of *m/z* 44 $[C_2H_6N]^+$ as N-protonated ethylideneamine (**27**) is in keeping with DFT calculations and labeling experiments. For example, H_2

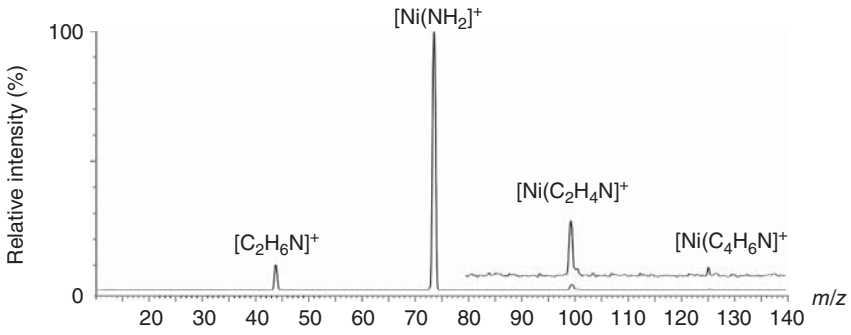

Figure 1.4 Mass spectrum resulting from the thermal reactions of mass-selected $[Ni(NH_2)]^+$ with C_2H_4 at a pressure of 0.9×10^{-4} mbar. The region between *m/z* 80 and 140 is enlarged by a factor 10. (Adapted from Ref. [28]. Copyright WILEY-VCH, **2012**.)

generated in reaction (1.13) contains one hydrogen atom from C_2H_4 and one from the amide group. Further, an intramolecular KIE of 1.4 has been determined for the reaction with CHD=CHD, and an effect of the stereochemistry in the reactions of **22** with *E*- and *Z*-CHD=CHD has not been observed.

In Figure 1.5, the PESs of the primary reactions for the ground and first excited states are depicted. Commencing with an electrophilic addition to form adduct complex **23**, the carbon-metal and carbon-nitrogen bonds are then formed via **TS 23/24** leading to **24**. Next, a sequence of two Ni-mediated H-atom shifts occur to first generate the metal hydride species **25**; then, passing through **TS 25/26** the complex **26** emerges that, upon liberation of atomic neutral Ni, generates $[CH_3CHNH_2]^+$ (**27**, *m/z* 44). In addition, complex **26** serves as a precursor for the dehydrogenation to form $[Ni(C_2H_4N)]^+$ (**30**) in a highly regioselective fashion. Details involve the oxidative insertion of the nickel atom in a N–H bond to produce the nickel hydride **28**. Molecular hydrogen is then generated in a σ-bond metathesis reaction via **TS 28/29** to produce **29** from which H_2 is liberated in a barrier-free dissociation. While the operation of a two-state reactivity (TSR) scenario is crucial in numerous reactions of cationic nickel complexes in the gas phase [3f, 29], in the systems described in Figure 1.5, it does not play a role, according to the calculations. For example, as shown in Figure 1.5a, there is no need to invoke the involvement of an excited singlet state in the generation of the main product pair $[CH_3CHNH_2]^+/^3Ni$. The reaction can smoothly proceed on the ground-state triplet surface. The same holds true for the dehydrogenation path, Figure 1.5b.

1.4 Conclusion and Perspectives

The studies discussed in this chapter exemplify how gas-phase reactions in conjunction with computational studies can shed light on often complex reaction